ELSEVIER

Journal of Structural Geology 28 (2006) 1483–1495

JOURNAL OF STRUCTURAL GEOLOGY

www.elsevier.com/locate/jsg

# Evidence of coseismic ruptures along the Roum fault (Lebanon): a possible source for the AD 1837 earthquake

Tony Nemer*, Mustapha Meghraoui

*EOST, Institut de Physique du Globe de Strasbourg (UMR 7516), 5 rue René Descartes, 67084 Strasbourg, France*

Received 13 July 2005; received in revised form 24 March 2006; accepted 30 March 2006
Available online 27 June 2006

**Abstract**

The Roum fault is the westernmost branch within the Lebanese restraining bend of the Dead Sea Transform Fault. This strike-slip fault extends for about 35 km from north of the Hula basin to the Awali river, and shows left-lateral strike-slip displacements (manifested as offset streams) and vertical movements. Recent seismic records indicate its seismogenic potential as the source of the double shock of 16 March 1956 (Ms 4.8, 5.1) earthquake. We studied the Roum fault using combined field investigations in geomorphology, structural geology, and palaeoseismology. Fresh fault scarps and pressure ridges visible along the fault trace attest to recent coseismic ruptures. A palaeoseismic trench investigation exposed a complex fault zone with several rupture strands and a minimum of four faulting episodes in the last ~10,000 years, the most recent event being post 84–239 AD. According to historical records, the 1 January 1837 (Ms 7.1) earthquake, which induced severe damage in the region, is the most likely candidate. Our results assign a slip-rate of 0.86–1.05 mm/year along the Roum fault, which shows that it accommodates about 14% of the total predicted strike-slip motion within the Lebanese restraining bend, and it should be considered a potential seismogenic fault for seismic hazard estimates in Lebanon.


*Keywords:* Roum fault; Historical earthquake; Dead Sea Transform; Palaeoseismology

## 1. Introduction

The Dead Sea Transform Fault (DSTF) is the continental plate boundary between the Arabia and Africa plates. It is an approximately 1000-km-long left-lateral strike-slip fault that connects the sea-floor spreading of the Red Sea in the south to the Arabia-Eurasia collision zone in the north (Fig. 1a). It can be subdivided into two sections trending north-south and joined by an approximately 170-km-long right-stepping bend that lies within the region known as the Lebanese restraining bend (Fig. 1a). Within this restraining bend, the DSTF splays into the through-going Yammouneh fault and four other subsidiary fault branches: the Roum, Hasbaya, Rachaya, and Serghaya faults (Fig. 1b). Of all these branches, the Roum fault (RF) is the only fault that has the same north-south trend of the southern section of the DSTF (Fig. 1), a fact which has led some authors to adopt the RF as the main continuation of the DSTF in Lebanon (e.g. Girdler, 1990; Butler et al., 1998). Other authors, however, have suggested that the Yammouneh fault is more likely to take up the majority of strain in the Lebanese restraining bend (e.g. Gomez et al., 2003; Daeron et al., 2004).

Based on tectonic, geodetic, and palaeoseismic studies, the relative plate motion along the DSTF has been estimated within a wide range of 1–10 mm/year (e.g. Quennell, 1958; Joffe and Garfunkel, 1987; Galli, 1999; McClusky et al., 2003; Meghraoui et al., 2003). However, the detailed geometry of splays of the DSTF within the Lebanese restraining bend and the related slip partitioning of the plate motion along the different fault branches have not been defined, apart from recent studies on the easternmost Serghaya fault (Gomez et al.,

* Corresponding author. Department of Geological Sciences, 101 Geological Sciences Building, University of Missouri, Columbia, MO 65211, USA. Tel.: +33 390 240 345; Fax: +1 573 882 5458.
*E-mail address:* nemert@missouri.edu (T. Nemer).

0191-8141/$ - see front matter © 2006 Elsevier Ltd. All rights reserved.
doi:10.1016/j.jsg.2006.03.038

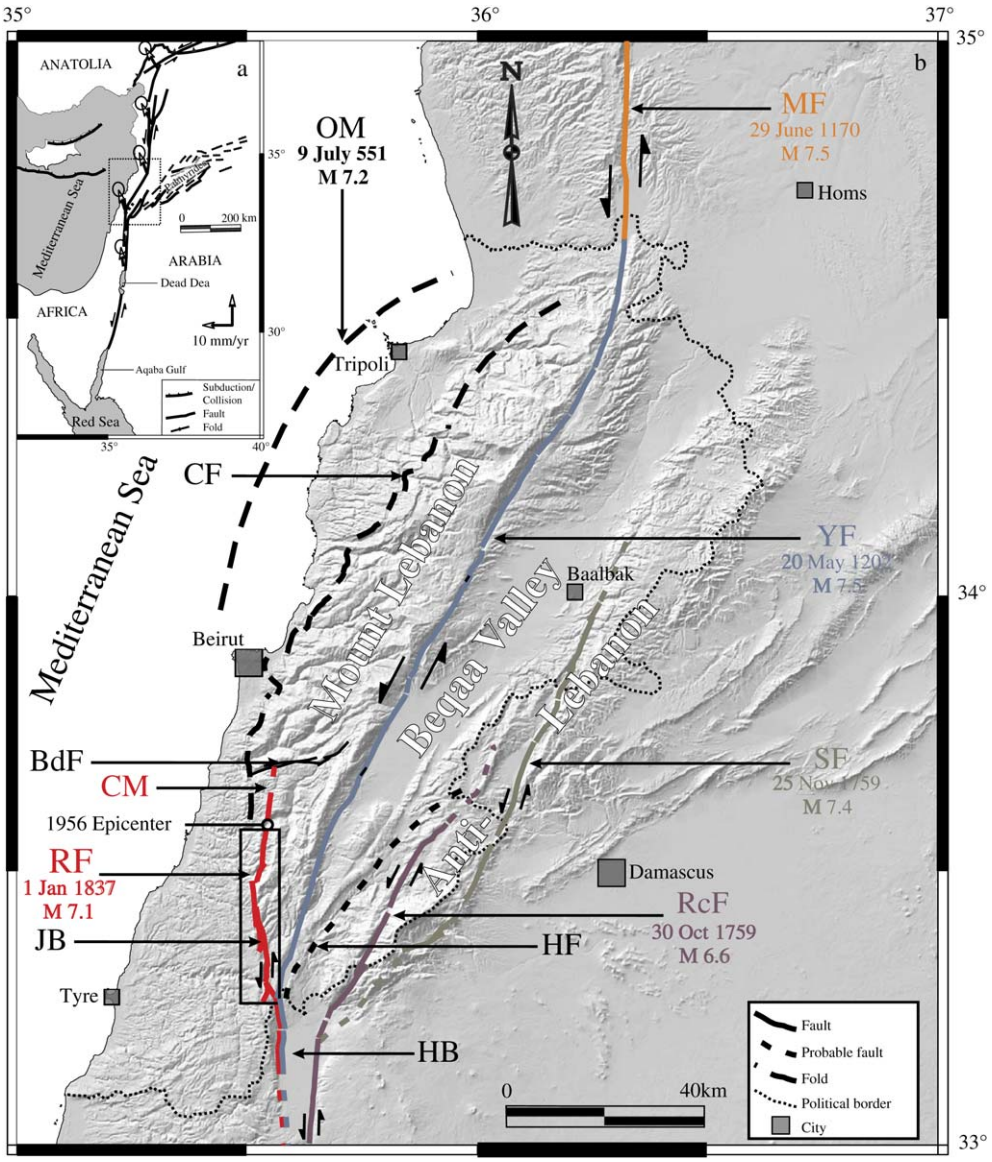


Fig. 1. (a) The Dead Sea Transform Fault extending from the Gulf of Aqaba to southeast Turkey. It is a left-lateral transform fault with a general N–S trend except in Lebanon where it bends rightward to form a restraining bend. Modified from McBride et al. (1990). Box shows location of b. White arrows indicate the GPS velocities of the Arabian plate relative to adjacent plates after McClusky et al. (2003). (b) Shuttle Radar Topography Mission 90-m-resolution digital elevation model of the Lebanese restraining bend showing the main units and structures: BdF, Beit-ed-Dine fault; CF, Coastal Flexure; CM, Chouf Monocline; HB, Hula basin; HF, Hasbaya fault; JB, Jarmaq basin; MF, Missyaf fault; OM, Offshore monocline; RcF, Rachaya fault; RF, Roum fault; SF, Serghaya fault; YF, Yammouneh fault. Note the epicentre location of the double-shock 1956 earthquake at the intersection between Roum fault and Chouf Monocline. Coloured faults are associated with large historical events (indicated by date and magnitude) that took place within the Lebanese restraining bend. Box around the Roum fault indicates location of Fig. 4a.

2003) and the through-going Yammouneh fault (Daeron et al., 2004).

In this paper, we focus on the structural geology, geomorphological and active tectonic expressions of the RF. Detailed field investigations and aerial-photograph analysis allow us to map the entire fault length, and show that it exhibits offset streams with faulted late Quaternary deposits along strike. Evidence of surface ruptures and fresh coseismic scarps that affect Holocene deposits implies a direct relationship to one or more of the major historical earthquakes that hit the region. Palaeoseismic investigations provide details on the past faulting activity and related earthquake recurrence along the RF. These results and the role of the RF are discussed within the framework of partitioning across the different strands of the DSTF in the Lebanese restraining bend.

## 2. Tectonic setting

The Lebanese restraining bend comprises two main mountain chains, the NNE-SSW trending Mount Lebanon and the NE-SW trending Anti-Lebanon, with the Beqaa Valley in between (Fig. 1b). This structural arrangement of two anticlinoria bounding a synclinorium (Hancock and Atiya, 1979) is a direct manifestation of the regional compression imposed

by the rightward bending of the left-lateral DSTF. Within the bend, and with the exception of the RF, the main faults have all a general NNE-SSW trend (Fig. 1b).

The limited detailed geological, structural, and bathymetric mapping of the Lebanese restraining bend and its associated offshore area has led several authors to suggest different tectonic scenarios taking place within the bend. In effect, Girdler (1990) traced the DSTF by combining the earthquake distribution and Landsat images, and found that the DSTF is consistent with a set of small circles centred about a 33° N, 24° E pole of rotation, and that the northernmost onshore small circle coincides with the RF. Butler et al. (1998) recorded several river offsets along the RF ranging from 200 m to 9 km and suggested that these are presumably underestimates of the total RF displacement. They estimated the total RF displacement on the basis of offset drainage basins, to be about 30 km (Butler et al., 1998). Other authors, however, suggest a limited extent of the RF based on field and remote sensing investigations (e.g. Griffiths et al., 2000; Khair, 2001). Griffiths et al. (2000) noted a decrease in surface expressions northward, defined the RF as a "lateral domain-bounding" fault accommodating the transpression of the Lebanese restraining bend, and suggested a fault tip to the south of Beirut. Khair (2001) proposed that the RF lateral displacement becomes dispersed beyond its mapped trace into a complex network of faults and fractures delineated as lineaments from aerial photographs.

The N–S trending RF extends for about 35 km from the western edge of the Hula pull-apart basin to the south and is subdued within inherited geological structures near the Awali river to the north. The RF is replaced immediately north of this river by a monoclinal structure, the Chouf Monocline, whose hinge extends along the same trend as the RF until the E–W Beit-ed-Dine fault (Figs. 1b, 2). To the north of this latter, a set of minor sub-latitudinal faults take place (Dubertret, 1955). To the west of the Chouf Monocline lies another monoclinal structure facing westward, the Coastal Flexure which may define together with the RF in the south, the western boundary of Mount Lebanon. The Coastal Flexure has a general hinge strike trending N–S (parallel to the RF) along its southern part and NNE–SSW (parallel to the Yammouneh fault) to the north of the latitude of Beirut (Fig. 1b).

## 3. The seismic activity and the 1837 earthquake

The instrumental seismicity (1903–2004; ISC, NEIC, EMSC bulletins) shows a scatter of moderate earthquake epicentres around the RF with one relatively important event, namely the double shock of 16 March 1956 (Ms 4.8, 5.1). Although earthquake location may be within a 10-km-error range in the absence of a reliable local seismic monitoring network in Lebanon, the epicentres of this double shock and its associated maximum damage were located near the northern tip of the RF (Plassard and Kogoj, 1981; Fig. 1b), suggesting this latter as a likely source.

According to the historical seismicity, two large events could be correlated with the RF: the 9 July 551 (Ms 7.2) earthquake that took place offshore Lebanon (Darawcheh et al., 2000) and the 1 January 1837 (Ms 7.1) earthquake that induced severe damage around the RF (Ambraseys, 1997; Fig. 1b). The 9 July 551 earthquake was a destructive event

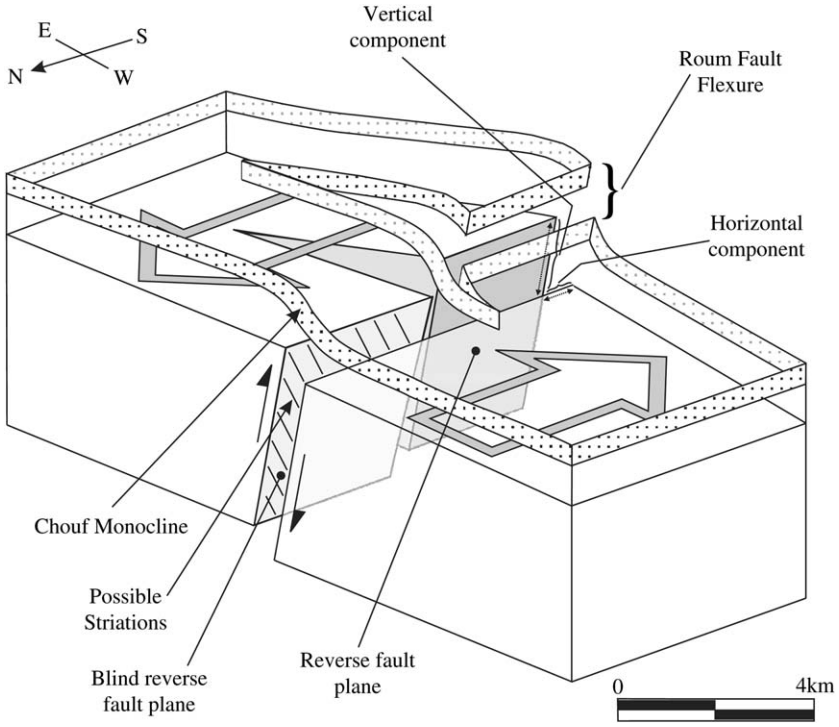


Fig. 2. Schematic block diagram showing the relationship between the Roum fault and the Chouf Monocline. Both structures overlie reverse faults: one blind leading to a simple monocline, and the other reaching the surface as a faulted monocline. Note that the vertical component is more prominent than the horizontal one along this segment of the Roum fault.

that affected the entire Lebanese coastal area and generated a Tsunami. Darawcheh et al. (2000), based on Byzantine documents, assessed a magnitude Ms of 7.1 to 7.3, proposed an epicentre location offshore Beirut, and correlated it with the nearby strike-slip RF. Such a correlation, however, implies an offshore continuation of the RF, an implication that lacks evidence of corresponding faulting along the coast and needs to be verified with detailed bathymetric investigations.

The 1 January 1837 earthquake was a large event with an epicentral area that extended from southern Lebanon to northern Israel (Fig. 3). A re-appraisal of this event was performed by Ambraseys (1997) based on local religious reports and some foreign consulate accounts, and suggests that it was probably a multiple event with the second shock occurring few minutes after the main one, and with three large aftershocks taking place few weeks later. From the damage distribution and an estimated Ms magnitude of 7.1, the source of these events was defined to be about 54 km in length and to be associated with the RF and its southern extension (Ambraseys, 1997; Fig. 3). However, even though this event seems to have been large enough to produce surface ruptures, no field observations have yet indicated that such ruptures exist (Ambraseys, 1997).

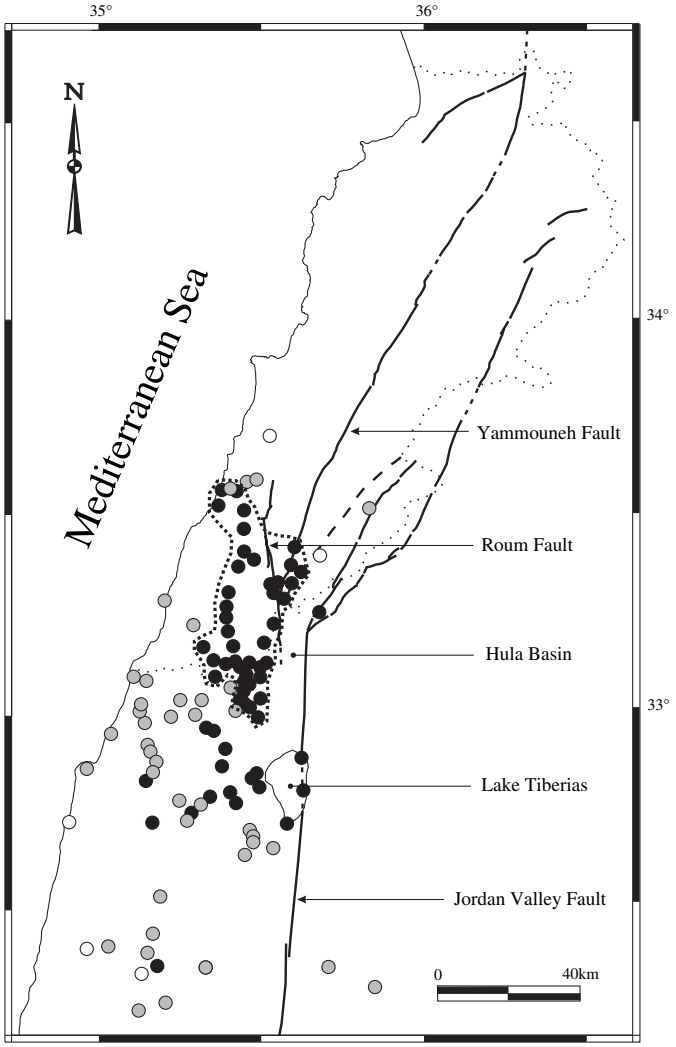


Fig. 3. The epicentral region of the 1837 earthquake (modified from Ambraseys, 1997). Circles indicate near-field locations of affected sites. Black, grey, and white circles correspond to MSK intensities of VIII, VII, and VI, respectively. Dotted contour bounds the area of concentrated maximum damage.

## 4. Structural and geomorphologic characteristics of the RF: evidence for late Quaternary faulting

Detailed mapping of the RF resulted from the analysis of 1:20.000-scale aerial photographs, a high-resolution (20 m/pixel) SAR digital elevation model, available geological maps (e.g. Dubertret, 1955), and field investigations. We note that the morphological and tectonic features along the active RF are different from the previously mapped fault (i.e. the geological fault).

As described by Dubertret (1955), the RF extends from the NW of the Hula basin striking NNW to follow the north-south trending Litani river valley and to continue northward until the Jarmaq basin (Fig. 1b). Further north, the RF continues along the western flank of Jabal Rafii until it reaches Jbaa where it gets replaced by a prominent flexure that extends north until the Awali river (Fig. 4a). Beyond this river, the Chouf Monocline takes over (Section 2, Fig. 2).

The cumulative displacement along the RF is not homogeneous along its length (Griffiths et al., 2000; Fig. 4b). Indeed, the horizontal component is more prominent along its southern segment (i.e. from Hula basin until Jbaa) and decreases northward. The associated drainage shows an overall left-lateral distributed shear and the valleys show consistent left-lateral offsets wherever they cross the fault trace. Due to restricted field access, these offsets were measured from the aerial photographs and their values are shown in Table 1. They range from small recent offsets (~7 m) to composite offsets (several kilometres), namely 8.5 km for the Litani river, 3.3 km for the Zahrani river, and 2.1 km for the Awali river (Fig. 4a,b). The homogeneous sinistral deflections within the low-relief sediment-filled Jarmaq basin attest for their tectonic control rather than topographic inheritance or erosional processes (Fig. 4a.). While the left-lateral component decreases to the north, the vertical component becomes more important (e.g. from Jbaa to the Awali river) and monoclinal flexure takes over (Fig. 4c). This deformation is typical of flexural-slip faulting that illustrates a combination and/or partitioning of strike-slip and contractional movements (Yeats et al., 1997).

The RF seems to bifurcate at the Litani river turn and shows two branches both lying to the west of the Beaufort castle (Fig. 4a). The western branch is the more evident and extends from the Litani river turn northwest toward the east of Yohmor and heads north toward Kfar-Tibnite where a gouge zone about 20 m wide is present in the vicinity of sub-vertical fault planes having strike-parallel striations and chatter marks indicating left-lateral displacement (Fig. 4d). From Kfar-Tibnite northward, the trace preserves its north-south trend and coincides with a fresh composite scarp (~2–3 m high; Fig. 5a) and elongated soft-sediment pressure ridges (~180 m long) following the scarp trend (Fig. 5b). These latter suggest young

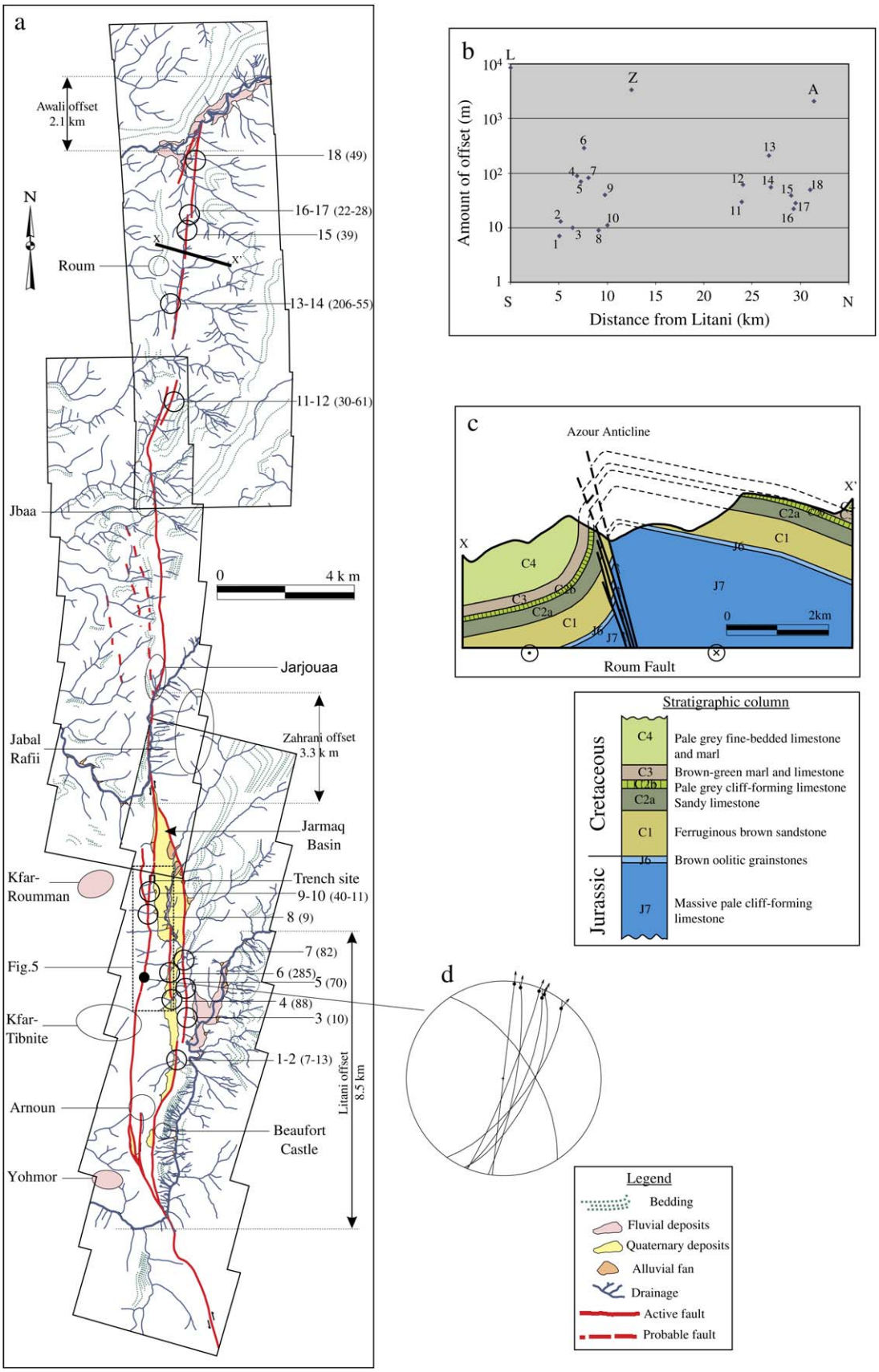


Fig. 4. (a) Trace of Roum fault area (location on Fig. 1b) based on field and aerial photograph mapping. Note the river offsets (thick blue) that decrease north. Labelled circles indicate places, numbered circles indicate drainage offsets plotted in b, numbers in brackets indicate offset length in m ± 2 (cf. Table 1). X−X′ is cross-section shown in c. Filled circle indicates the location of the kinematic measurements shown in d. (b) Log-normal plot of offset drainage distribution along the Roum fault from south to north as shown in a. Note that the cumulative offsets recorded by the Litani (L), Zahrani (Z), and Awali (A) rivers decrease northward. Numbers indicate the offset labels given in Table 1. (c) Cross-section drawn to scale along the flexing segment of Roum fault. (d) Stereographic projection of fault planes and corresponding slickenlines measured along the Roum fault at N33°21′.71−E35°31′.35 shown in a. The rake points out the strike-slip movement along this segment of the Roum fault.

Table 1
River- and stream-offset distribution and estimated ages along the RF

| Offset name/label | Along-strike distance from Litani river's offset (km) | Offset length in m (±2) | Estimated age range (ky) = offset ÷ slip rate |
|---|---|---|---|
| Litani | 0.0 | 8500 | 8095–9884 |
| 1 | 5.0 | 7 | 7–8 |
| 2 | 5.2 | 13 | 12–15 |
| 3 | 6.5 | 10 | 9–12 |
| 4 | 6.9 | 88 | 84–102 |
| 5 | 7.3 | 70 | 66–81 |
| 6 | 7.6 | 285 | 271–331 |
| 7 | 8.1 | 82 | 78–96 |
| 8 | 9.1 | 9 | 9–11 |
| 9 | 9.7 | 40 | 38–47 |
| 10 | 10.0 | 11 | 11–13 |
| Zahrani | 12.5 | 3309 | 3151–3848 |
| 11 | 23.9 | 30 | 29–35 |
| 12 | 24.0 | 61 | 58–71 |
| 13 | 26.7 | 206 | 196–239 |
| 14 | 26.9 | 55 | 52–64 |
| 15 | 29.0 | 39 | 37–45 |
| 16 | 29.3 | 22 | 21–25 |
| 17 | 29.5 | 28 | 26–32 |
| 18 | 31.0 | 49 | 47–57 |
| Awali | 31.4 | 2087 | 1988–2427 |

The numbers in the first column indicate the stream labels shown in Fig.4. The distances from the Litani river and the offset lengths are determined from air photos. The ages are inferred from the estimated slip rate of 0.86–1.05 mm/year (offset ÷ slip rate), which correspond to the age of fault offset record at each point.

fault movements (probably Late Pleistocene) as otherwise they would have been eroded under the prevailing Mediterranean climate of Lebanon with mild summers and wet winters, where the average annual temperature value is about 18 °C and the average precipitation rate of the study area is about 1000 mm/year (Atlas climatique du Liban, 1988). Similar structures have been observed after the 1999 Izmit earthquake in Turkey, with mole tracks and pressure ridges as surface faulting (Barka et al., 2002). Further north, the western branch continues into the north-western part of the Jarmaq basin toward the Zahrani river valley. The eastern branch extends from the Litani river turn NNW and then north toward the west of the Beaufort castle where it bounds several north–south trending quaternary basins (Fig. 4a). It continues north to form the eastern edge of the Jarmaq plain, at the north of which it joins the aforementioned western branch.

The presence of the Jarmaq plain between the two southern branches of the RF, together with its relatively low relief with respects to its surroundings, suggests that this plain might be a pull-apart basin (Butler et al., 1998; Griffiths et al., 2000). Its Miocene and Quaternary deposits indicate that the associated extensional regime goes back to Miocene times and has continued ever since.

To the north of the Jarmaq basin, the RF trace is less straightforward. It joins the north-south trending Zahrani river valley. Further north, it bifurcates, with the eastern splay heading north toward Jbaa and coinciding with several gouge zones present along its trend. To the north of Jbaa, the RF structural behaviour becomes somehow more complicated as its vertical component becomes more pronounced and the faulting is manifested as a flexure (Fig. 4c). It must be noted, however, that along the above delineation of the RF no evidence of tectonic creep was observed, which suggests a seismic behaviour of the RF.

## 5. Palaeoseismic analysis

Even though we located several places as good potential palaeoseismic trenching sites, our investigations were restricted by the existence of the indiscriminately sown land mines in southern Lebanon, which rendered our work possibilities very limited. However, we excavated an active fault branch along the western edge of the Jarmaq basin where the fault affects recent colluvium and older sedimentary deposits (Fig. 5c).

We made use of an already opened 10-m-long cultivation excavation that made an angle of 60° with the fault trend. Only the southern wall was preserved, which we deepened down to 3 meters, and exposed several intermittent colluvial and caliche horizons (Fig. 6a). The exposure presented clearly faulted sedimentary units, 6 out of 7 (*a*–*g*), with well developed stratigraphy.

- At the bottom lies unit *g* which consists of a massive white caliche with few scattered limestone pebbles. This unit is truncated east and west by the different shear zones.
- Unit *h* lies to the west of unit *g* where they are separated by a fault branch. It is made up of a brown soil matrix containing poorly sorted limestone clasts that have a defined fabric extending parallel to the shear zone, together with some sheared caliche-derived material.
- Unit *f* overlies unit *g* and corresponds to a colluvial deposit made up of brown sandy soil matrix with brecciated and poorly sorted gravels. This unit shows a dramatic increase in thickness to the west, which varies from 10 cm to about 1.5 m, and is truncated to the east (where it is referred to as *f1*) by a listric normal fault that is inferred from the down-dip differential offsets *d1*/*d1*, *e1*/*e1* and *f*/*f1* (Fig. 6).
- Unit *e* is another caliche layer with a beige colour and containing rounded limestone pebbles. It is also truncated to the east where it becomes less compact (referred to as *e1*). Block *e2* is a brecciated and reconsolidated block, originally of unit *e*.
- Unit *d* is a light-brown sandy layer about 20- to 30-cm thick that overlies unit *e*. It is not continuous, since it gets affected by the various shear zones whereby it gets lost to the west and becomes more friable to the east (unit *d1*) above unit *e1*.
- Unit *j* is a post-seismic colluvial wedge made up of highly unsorted material (up to 1-m-long limestone boulders) and sandwiched between units *d1* and *c*.
- Unit *c* is a dark brown silty soil, about 40 cm thick, and contains few large well-rounded limestone cobbles. A thin layer of intermittent pebbles separates it from unit *d* below, and it is fault-affected east and west as well.

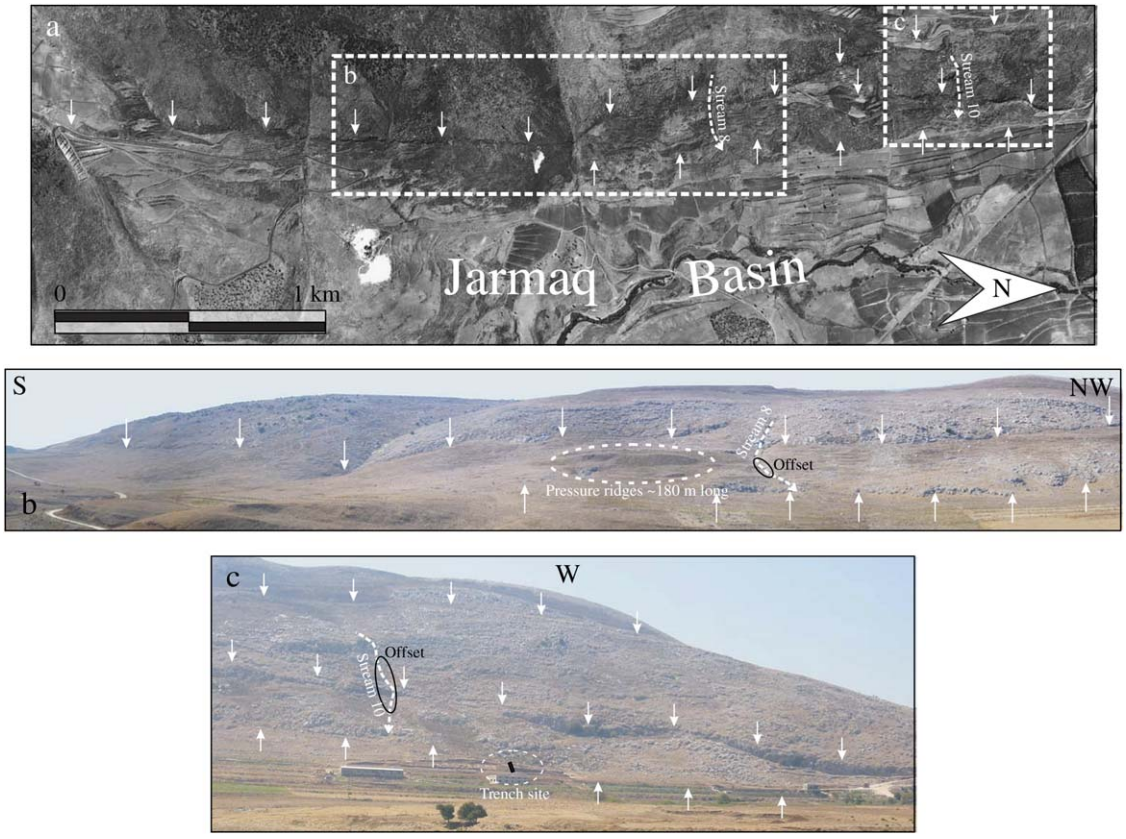


Fig. 5. (a) Aerial photograph showing the Roum fault to the west of Jarmaq basin (see location on Fig. 4). Fault trace(s) indicated with white arrows. Boxes indicate locations of b and c. (b) Field photograph showing fresh composite fault scarps (2–2.5 m high) indicated with white arrows and offset stream (labelled 8 on Fig. 4 and in Table 1). Note also the pressure ridges between the two fault scarps. (c) Field photograph showing trench location and offset stream 10 (Fig. 4 and in Table 1). Fault trace(s) are indicated with white arrows.

- Unit *b* is about 40 cm thick and consists of densely distributed limestone pebbles within a sandy brown soil matrix. This unit is the last layer affected by faulting and consequently may be defined as the last event horizon.
- Unit *a* is the uppermost layer that corresponds to the capping layer and the present plough zone.

The excavation reveals several shear zones that affect the different sedimentary units, and which show a significant normal component ($\sim$50 cm), as indicated for instance to the east by the offset units *d*, *e*, and *f* and by the presence of the colluvial wedge *j*. Moreover, strike-slip movements are also indicated by the clear sets of shear fabric aligned along the different fault zones and by the presence of detached faulted blocks (e.g. block *e2*) and sheared material (unit *h*). The intense deformation is inferred from the different sets of shear fabric that are aligned along the different shear zones and capped by the appropriate capping layers; and as the shear fabric is characteristic of coseismic movement, the corresponding palaeo-earthquakes were inferred to be surface rupture events with magnitudes Ms $>$ 6.5.

Ten samples (5 detrital charcoals and 5 bulk soils) were collected for radiocarbon dating. They were processed at Christian-Albrechts-Universität of Kiel, Germany, using $^{14}$C accelerator mass spectrometry (AMS). The results (Table 2) reveal that 6 samples gave enough carbon to be dated, with one sample (JAR-7) reflecting a modern age (post AD 1954) probably due to some reworking contamination, and another sample (JAR-14-B) having little carbon and therefore reflecting a less reliable result. The other four (JAR-1-B, JAR-2-B, JAR-13-B, and JAR-17-B) have normal-range $\delta^{13}$C values and their dates can be considered reliable. It should be noted, however, that sample (JAR-17-B) of block *e2* gives a younger age than sample (JAR-13-B) of unit *e*, probably as a result of the reworking of unit *e* to lead to *e2* (brecciation and reconsolidation). Constraints on the timing of the palaeoseismic events are provided by considering the stratigraphic superposition of the different layers and applying a Bayesian analysis (conditional probability for the stratigraphic succession and dating; Bronk Ramsey, 1998) to the age ranges obtained from calibration of the radiocarbon ages (Fig. 7).

Five seismic events were inferred from the fault branch distribution and their cross-cutting relationships with the different sedimentary units and event horizons as illustrated in Fig. 6. A reconstruction of these events together with the stratigraphic deposition is shown in Fig. 8:

Event *Z* this is the most recent event that affected the entire units except unit *a* which caps and postdates the faulting event (Fig. 8). The date of this event may

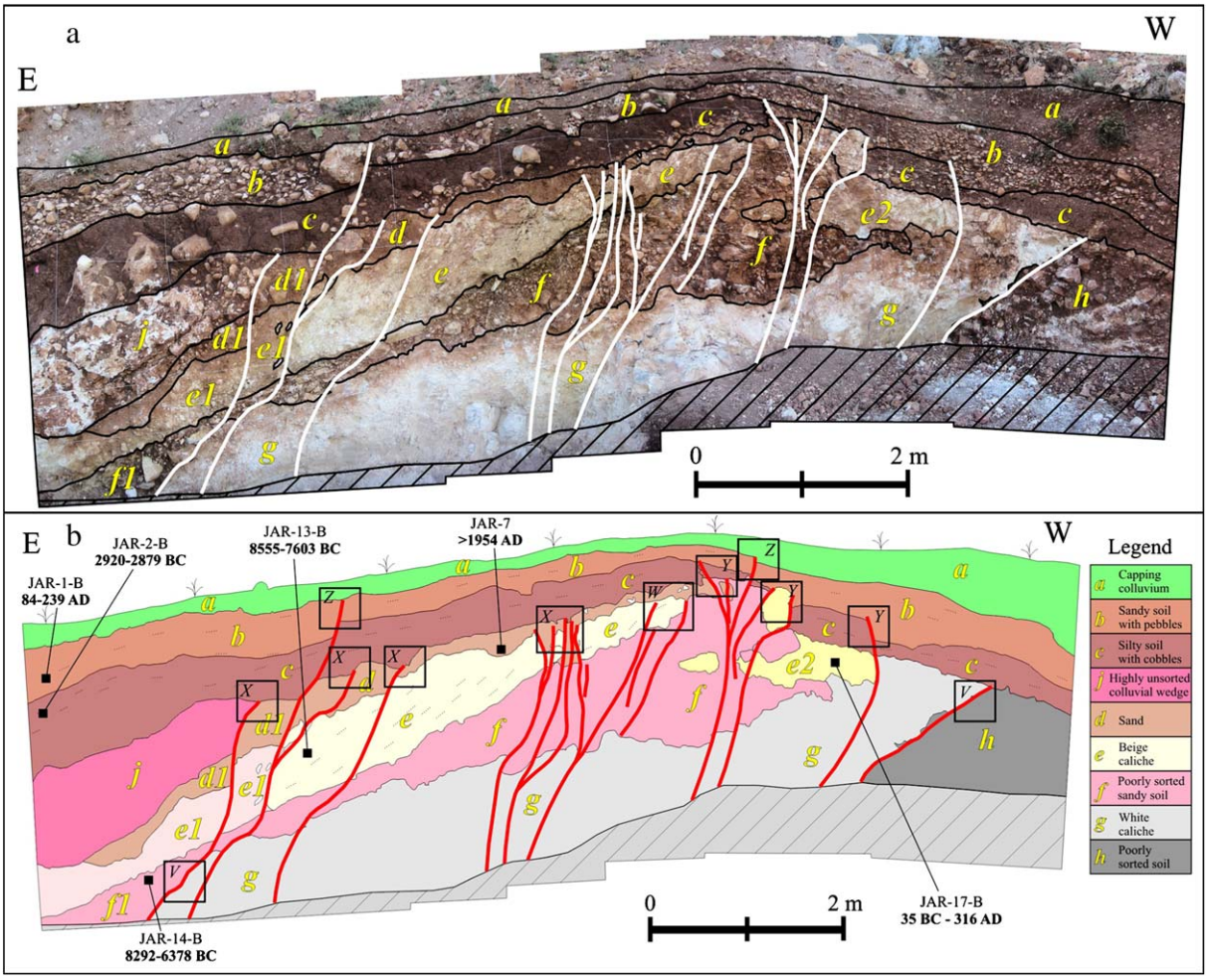


Fig. 6. (a) Photo mosaic of the southern wall of the excavation across the Roum fault showing the rupture strands (white lines) and associated stratigraphic units (labelled in yellow). (b) Illustration of a. The 5 palaeoseismic events determined from the capping horizons are labelled *V* to *Z* in black boxes (see text for details and Fig. 7 for the palaeo-earthquake distribution). Black squares are the 6 measured and reliable unit radiocarbon ages.

be inferred from the age of the last affected unit (unit *b*), which dates to 84–239 AD, and subsequently event *Z* must have occurred after that date (Fig. 7).

Event *Y* the penultimate event seems to have ruptured up to unit *c* and is covered by unit *b*, which constrains this event date between the ages of units *c* and *b*, i.e. between 2920–2879 BC and 84–239 AD (Figs. 6–8).

Event *X* this event occurred before the deposition of unit *c* (i.e. pre 2920–2879 BC) whereby it clearly affects unit *d* and led to the formation of a fault scarp at which abuts the colluvial wedge *j* (Figs. 6, 8). However, in the absence of an age range for unit *d* (modern age, Table 2), which otherwise would provide an event date constrained between the ages of units *d* and *c*, this event may be defined within the large age bracket between units *e* and *c*, and therefore between 8555–7603 BC and 2920–2879 BC (Fig. 7).

Event *W* this event took place before the deposition of unit *d* whereby unit *e* is truncated and overlain by unit *d* (Figs. 6, 8). This event would be constrained between units *e* and *d*, but for the same reason concerning unit *d* mentioned above, it is like event *X* constrained between units *e* and *c*, although it predates event *X* (Fig. 7).

Event *V* the oldest event detected in the excavation likely took place before the deposition of unit *f* whereby it truncates unit *g* east and west and seems to have affected the excavation margins (Figs. 6, 8). However, in the absence of a reliable age of unit *f* (Table 2), event *V* cannot be correlated with this unit but instead with the closest dated unit (unit *e*), and subsequently it is pre 8555–7603 BC.

## 6. Discussion

Detailed mapping of the 35-km-long RF shows definite evidence of surface faulting along its trace, namely gouge zones, fresh fault scarp, pressure ridges, and deflected streams. Moreover the palaeoseismic excavation reveals the presence of several shear zones and offset sedimentary units with intense

Table 2
Characteristics of the radiocarbon dating of the collected samples

| Sample name | Sample Lab ID | Material | Sampled layer | Amount of carbon (mg) | Current (% of 1 mg sample) | $\Delta\ ^{13}C$ (‰) | Radiocarbon age (BP) | 2σ calibrated age range | Lab remark on result |
|---|---|---|---|---|---|---|---|---|---|
| JAR-1-B | KIA25533 | Bulk soil | *b* | 4.55 | 96 | $-23.76 \pm 0.07$ | $1848 \pm 26$ | 84–239 AD | Good |
| JAR-2-B | KIA25534 | Bulk soil | *c* | 1.31 | 98 | $-23.66 \pm 0.19$ | $4287 \pm 27$ | 2920–2879 BC | Good |
| JAR-5 | KIA25535 | Charcoal | *g* | 0.02 | Not reduced | n/a | n/a | n/a | No gas/material left |
| JAR-7 | KIA25536 | Charcoal | *d* | 0.52 | 93 | $-27.70 \pm 0.17$ | Modern | Post 1954 AD | Good |
| JAR-11 | KIA25537 | Charcoal | *f* | 0.01 | Not reduced | n/a | n/a | n/a | No gas/material left |
| JAR-13-B | KIA25538 | Bulk soil | *e* | 0.21 | 48 | $-29.90 \pm 0.26$ | $8982 \pm 193$ | 8555–7603 BC | OK |
| JAR-14-B | KIA25539 | Bulk soil | *f1* | 0.08 | 15 | $-31.49 \pm 0.22$ | $8306 \pm 425$ | 8292–6378 BC | ± Reliable |
| JAR-15 | KIA25540 | Charcoal | *e1* | 0.01 | Not reduced | n/a | n/a | n/a | No gas/material left |
| JAR-16 | KIA25541 | Charcoal | *f* | 0.00 | Not reduced | n/a | n/a | n/a | No gas/material left |
| JAR-17-B | KIA25542 | Bulk soil | *e2* | 0.35 | 77 | $-27.64 \pm 0.44$ | $1890 \pm 63$ | 35 BC–316 AD | Good |

All dating methods are AMS. The sampled layers are illustrated in Fig. 6. The calibrated ages are according to "CALIB rev 4.3" (Stuiver and Reimer, 1993) using the calibration curves of Stuiver et al. (1998). The adopted age ranges are equivalent to the 2σ age ranges (95.4% density). n/a, not available.

shear fabric, which attests that the fault is capable of generating large earthquakes. The palaeoseismic investigation revealed that the most recent seismic event postdates 84–239 AD and could be correlated, based on the historical record, with either the 9 July 551 earthquake or that of 1 January 1837. However, since the former seems to have an offshore epicentre and large damage along the coast (Darawcheh et al., 2000) with relatively less damage inland, and the latter had a severe damage distribution in the vicinity of the mapped RF (Section 3; Fig. 3), we believe that the 1837 earthquake is more likely to correspond to the most recent detected event. Such an inference is mainly based on the wealth of the historical documents of the eastern Mediterranean region where several historical studies have been conducted, and subsequent parametric catalogues have been published (e.g. Poirier and Taher, 1980; Plassard and Kogoj, 1981; Ben-Menahem, 1991; Ambraseys et al., 1994; Sbeinati et al., 2005). These catalogues span altogether the period 1365 BC–1927 AD and may be considered complete for magnitude greater than 6.5 for the last 2000 years (e.g. Sbeinati et al., 2005).

It could be argued that the intensity distribution of Fig. 3 correlates as well with the southern part of the Yammouneh fault and its southern extension in northern Israel, but the lack of evidence of destruction to the east of the Jordan Valley and Yammouneh faults, and the fact that damage is concentrated to the west of these faults and the RF, make of this latter

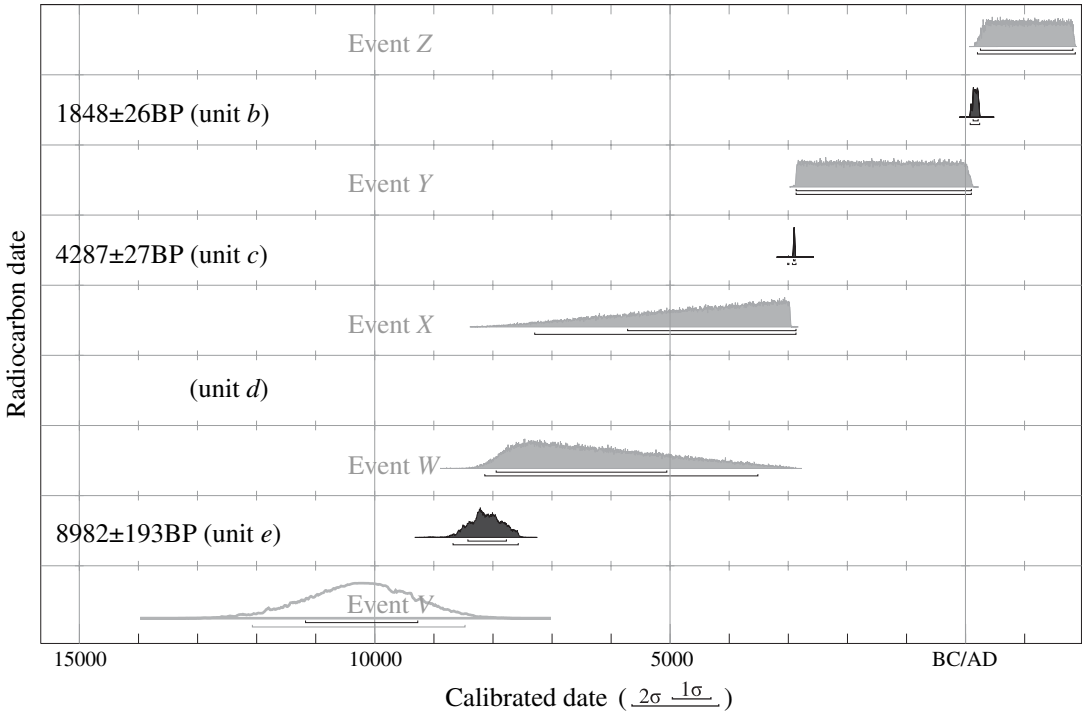


Fig. 7. Probability distribution of $^{14}C$ ages (Table 2) obtained from sequential radiocarbon dates automatically performed by the OxCal 3.10 Program (Bronk Ramsey, 1998; http://www.rlaha.ox.ac.uk/O/oxcal.php). The calibrated dates (black) are presented with 1σ and 2σ age ranges (68.3% and 95.4% density, respectively). The age ranges of the seismic events (grey) are determined using the Bayesian distribution and related conditional probability imposed by the stratigraphic sequence, event horizons and $^{14}C$ dating. Event *V* is, however, poorly constrained without the lower bound age.

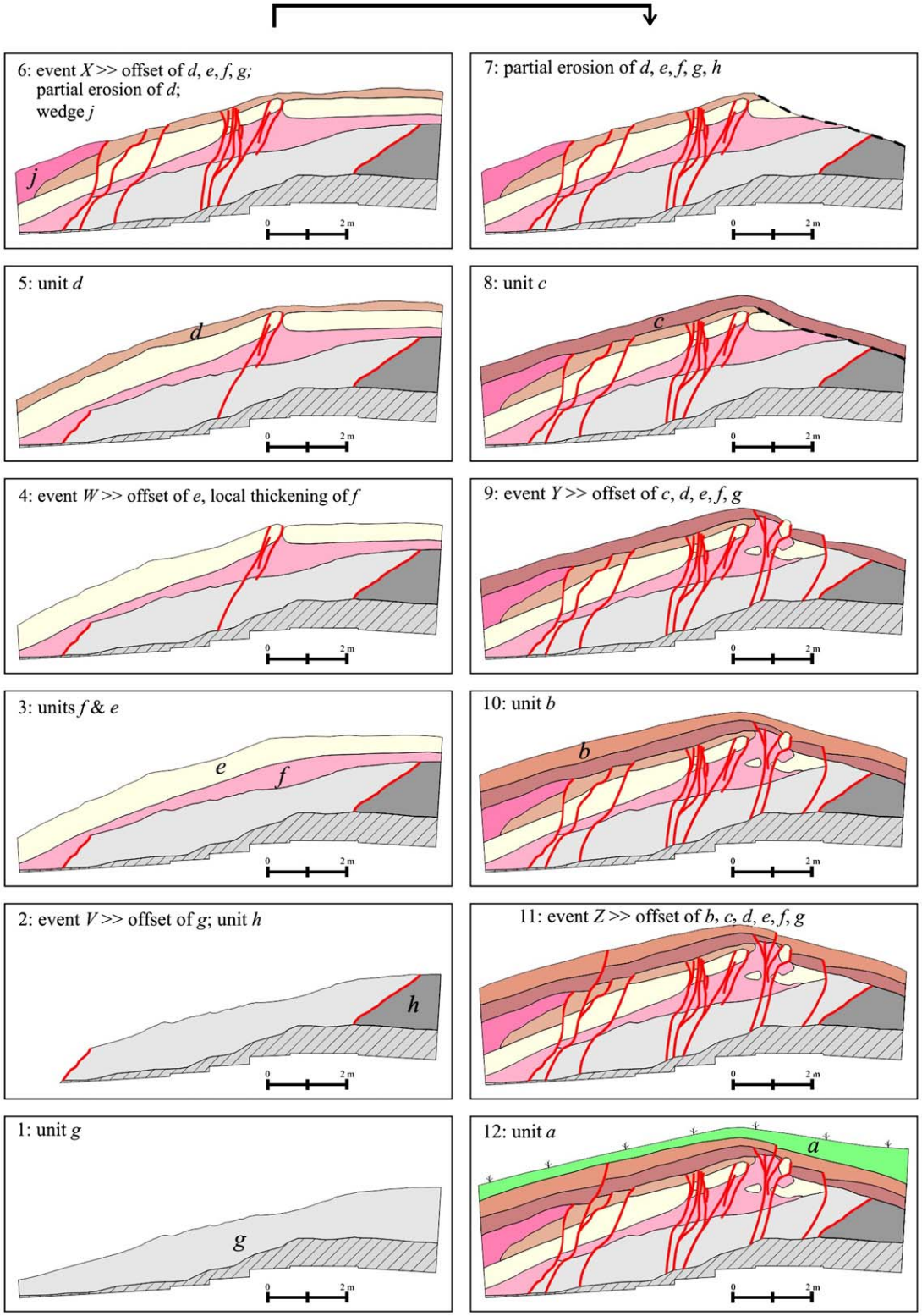


Fig. 8. Schematic reconstruction of the palaeoseismic events as observed in the trench (Fig. 6a). Steps 1 to 12 illustrate the relationships between the 5 faulting episodes and successive alluvial-colluvial deposits. The white caliche units ( *g* and *e*) mark the stratigraphic succession and point out the rupture locations. Event *Z* is covered by unit *a*, which corresponds to a thick colluvial unit visible on the western edge of the trench.

the most likely candidate of being the source of the 1837 earthquake (Fig. 3; Section 3). The 54-km rupture length of the source of the 1837 earthquake must be accounted for by the RF and its southern extension as proposed by Ambraseys (1997). However, the southern extension(s) which bound(s) the Hula basin, lack(s) the appropriate evidence of being a segment of the RF or of the Yammouneh fault as both faults bifurcates from the DSTF to the north of the Hula basin.

Moreover, this segment seems to have ruptured with the Yammouneh fault during the May 20, 1202 (Ms 7.5) earthquake as shown by Ellenblum et al. (1998) and Daeron et al. (2005). Accordingly, the tectonic behaviour of this segment of the DSTF remains to be clarified as it requires further investigations in view of the several associated historical earthquakes.

The time distribution of the detected seismic events is as follows: event *V* predates 8555–7603 BC, events *W* and *X* lie between 8555–7603 BC and 2920–2879 BC, event *Y* lies between 2920–2879 BC and 84–239 AD, and event *Z* postdates 84–239 AD, which correspond to four seismic events postdating 8555–7603 BC and taking place during the last 10510 years. The 54-km rupture length of the RF during the 1837 earthquake (Ambraseys, 1997) can produce an average lateral surface displacement of about 1m using the scaling laws of Wells and Coppersmith (1994). However, the coseismic lateral slip along such a rupture length can be up to 5 m as observed during the 12 November 1999 (Mw 7.1) Düzce earthquake in Turkey (Akyuz et al., 2002). If we are to relate our palaeoseismic observations to the geomorphic offset markers, the smallest offset streams that are closest to the excavation site (i.e. the streams labelled 8 and 10 in Figs. 4a and 5b,c) may be incising at the surface the relatively competent caliche units that are exposed at the base of the excavation (units *e* and *g* in Fig. 6). If this is the case, the 9–11 m of left-lateral stream offsets (Table 1) may have been accumulated through coseismic displacements during the last 10,510 years, which corresponds to a slip rate of 0.86–1.05 mm/year and to an average surface rupture of 2.5 m per event. Such a slip rate can account for about 14% of the total predicted strike-slip motion of 6.8 mm/year within the Lebanese restraining bend (McClusky et al., 2003; Nemer, 2005; Gomez et al., 2006).

By extrapolating this slip rate into all the drainage offsets, we can estimate a minimum age for each offset (Table 1), and from the largest offset (8.5 km), we may infer that the RF has been active since at least 8.5 Myr, which fits well with the presence of Miocene sediments within the Jarmaq pull-apart basin (Section 4). As to the northern offsets (e.g. the 2.1 km of the Awali river), their relatively younger ages based on the 0.86–1.05 mm/year may be due to two different scenarios: (1) the fault is propagating north and has a constant slip-rate, whereby the estimated ages can provide a constraint to the propagation rate, that is 0.22 mm/year; (2) the fault has a fixed length and the slip rate is decreasing to the north, whereby the younger ages are a function of applying higher values of slip rate to the northern part of the fault (if we assume a more or less the same age of the corresponding topography, i.e. of the drainage incision). Since from the current dataset we cannot differentiate between the two scenarios, the decrease in the horizontal displacement that is contemporaneous with the increase in the vertical one northward along the RF should be borne in mind, as this is not uncommon within positive flower structures which may well be the case of the Lebanese restraining bend (Davis and Reynolds, 1996). However, additional studies are needed to derive better constrained slip-rate estimates along the strike of the RF, to test whether or not the fault is propagating northward, to date the offset geomorphic markers (e.g. fans, terraces) along the different segments of the fault, to correlate the ages of these markers with the long-term climatic changes, and to clarify the tectonic scenario induced by the fault branching (Cowie and Roberts, 2001; Morewood and Roberts, 2002).

Within the Lebanese restraining bend, the RF represents the southwestern boundary of the wedge-shaped block limited to the east by the Yammouneh fault (Griffiths et al., 2000; Fig. 1b). The confinement of this block between these two faults has resulted in a relatively uplifted structure that constitutes the southern part of Mount Lebanon. This uplift and the regional strike-slip movement are both manifested along the RF, with the horizontal movement being more important in the south, and vertical movement taking over in the north (Fig. 2). To the north of the Awali river, the Chouf Monocline seems to represent the northern continuation of the RF. This monoclinal structure most probably overlies a reverse blind fault which may well be the northern continuation of the RF (Fig. 2). Similarly, the Coastal Flexure likely overlies another reverse blind fault. These blind faults are driven by the contractional movement along the Lebanese restraining bend, and are most probably lateral ramps to the main Yammouneh fault. Based on this, and in the absence of faulting evidence along the coast and of detailed bathymetric surveys that may enhance our knowledge about any offshore structures, the direct correlation of the RF with the 9 July 551 offshore earthquake (Darawcheh et al., 2000) remains speculative and has to take into account this lateral-ramp geometry. However, we suspect that a structure similar to the Coastal Flexure lies offshore Lebanon and is probably controlled by another blind reverse fault, i.e. another lateral ramp that connects with the Yammouneh fault. This structure, indicated in Fig. 1 as the Offshore Monocline, was most probably the source of the 9 July 551 Ms 7.2 earthquake. Offshore investigations are definitely needed to confirm its presence.

## 7. Conclusion

We studied the RF using combined field investigations in geomorphology, structural geology, and palaeoseismology. Detailed mapping reveals that it is limited in extent to about 35 km from north of the Hula basin to the Awali river. It is associated with the presence of fresh fault scarps and pressure ridges along its strike, and with two sub-parallel fault branches that bound the Miocene Jarmaq pull-apart basin in the south. Small and large cumulative left-lateral drainage offsets were observed, together with vertical movements that become more important along the northern segment of the fault.

Recent seismic records indicate the seismogenic potential of the RF as the source of the double shock of 16 March 1956 (Ms 4.8, 5.1) earthquake. Our palaeoseismic study confirms that the RF is an active seismogenic structure: it shows the occurrence of at least 4–5 large seismic events with surface ruptures during the last 10510 years, the last event being post 84–239 AD (Figs. 6–8). We believe that the 1 January

1837 (Ms 7.1) earthquake, which induced severe damage in the region, is the most likely candidate for being the most recent large seismic event along the RF. A slip-rate of 0.86–1.05 mm/year was derived, which indicates that the RF accommodates about 14% of the total predicted strike-slip motion within the Lebanese restraining bend.

The RF constitutes a local branch of the DSTF that is one of the most important but relatively poorly known fault systems in the world in terms of recent tectonic activity and palaeoseismic evolution. Our study aimed to shed partial light on this plate boundary, which requires further and extensive active tectonic and palaeoseismic research. The potential of the RF for producing large earthquakes similar in magnitude to that of 1837 must be taken into consideration within any seismic hazard study of the region, bearing in mind that further field studies along the fault and its associated structures (i.e. Chouf Monocline and southern extension) are needed for a more comprehensive assessment of their seismogenic potential.

## Acknowledgements

This research was supported by the APAME EC project (ICA3-CT-2002-10024). We thank J. van der Woerd (Institut de Physique du Globe de Strasbourg) for fruitful comments on the drafts, F. Gomez for topographic data, and R. Sbeinati and I. Layyous (Syrian Atomic Energy Commission) for field assistance. We are grateful to M.-J. Nadeau and P. Grootes (Christian-Albrechts-Universität of Kiel) for the radiocarbon dating results and comments. We owe H. Nabhan great thanks for allowing the excavation of his land. We also thank Z. Shipton and an anonymous reviewer for helpful reviews of the manuscript.

## References

Akyuz, H.S., Hartleb, R., Barka, A., Altunel, E., Sunal, G., Meyer, B., Armijo, R., 2002. Surface rupture and slip distribution of the 12 November 1999 Duzce earthquake (*M* 7.1), North Anatolian Fault, Bolu, Turkey. Bulletin of the Seismological Society of America 92, 61–66.

Ambraseys, N.N., 1997. The earthquake of 1 January 1837 in southern Lebanon and northern Israel. Annali di Geofisica 40, 923–935.

Ambraseys, N.N., Melville, C.P., Adams, R.D., 1994. The Seismicity of Egypt, Arabia and the Red Sea: A Historical Review. Cambridge University Press.

Atlas climatique du Liban, 1988. Ministère des travaux publics, Liban.

Barka, A., Akyüz, H.S., Altunel, E., Sunal, G., Çakır, Z., Dikbaş, A., Yerli, B., Armijo, R., Meyer, B., Chabalier, J.B., Rockwell, T., Dolan, J.R., Hartleb, R., Dawson, T., Christofferson, S., Tucker, A., Fumal, T., Langridge, R., Stenner, H., Lettis, W., Bachhuber, J., Page, W., 2002. The surface rupture and slip distribution of the August 17, 1999 İzmit earthquake, M = 7.4, North Anatolian Fault. Bulletin of the Seismological Society of America 92, 43–60.

Ben-Menahem, A., 1991. Four thousand years of seismicity along the Dead Sea rift. Journal of Geophysical Research 96, 20195–20216.

Bronk Ramsey, C., 1998. Radiocarbon Calibration and Analysis of Stratigraphy: the OxCal Program. Radiocarbon 37, 425–430.

Butler, R.W.H., Spencer, S., Griffiths, H.M., 1998. The structural response to evolving plate kinematics during transpression: evolution of the Lebanese restraining bend of the Dead Sea transform. In: Holdsworth, R.E., Strachan, R.A., Dewey, J.F. (Eds.), Continental Transpressional and Transtentional Tectonics, Special Publications, 135. Geological Society, London, pp. 81–106.

Cowie, P.A., Roberts, G.P., 2001. Constraining slip rates and spacings of active normal faults. Journal of Structural Geology 23, 1901–1915.

Daeron, M., Benedetti, L., Tapponnier, P., Sursock, A., Finkel, R.C., 2004. Constraints on the post ~25-ka slip rate of the Yammouneh fault (Lebanon) using in situ cosmogenic $^{36}$Cl dating of offset limestone-clast fans. Earth and Planetary Science Letters 227, 105–119.

Daeron, M., Klinger, Y., Tapponnier, P., Elias, A., Jacques, E., Sursock, A., 2005. Sources of the large A.D. 1202 and 1759 Near East earthquakes. Geology 33, 529–532.

Darawcheh, R., Sbeinati, M.R., Margottini, C., Paolini, S., 2000. The 9 July 551 AD Beirut earthquake, eastern Mediterranean region. Journal of Earthquake Engineering 4, 403–414.

Davis, G.H., Reynolds, S.J., 1996. Structural Geology of Rocks and Regions. John Wiley and Sons..

Dubertret, L., 1955. Carte géologique du Liban avec notice explicative. République Libanaise, Ministère des travaux publics. scale 1:200,000.

Ellenblum, R., Marco, S., Agnon, A., Rockwell, T., Boas, A., 1998. Crusader castle torn apart by earthquake at dawn, 20 May 1202. Geology 26, 303–306.

Galli, P., 1999. Active tectonics along the Wadi Araba-Jordan Valley transform fault. Journal of Geophysical Research 104, 2777–2796.

Girdler, R.W., 1990. The Dead Sea transform fault system. Tectonophysics 180, 1–13.

Gomez, F., Meghraoui, M., Darkal, A.N., Hijazi, F., Mouty, M., Suleiman, Y., Sbeinati, R., Darawcheh, R., Al-Ghazzi, R., Barazangi, M., 2003. Holocene faulting and earthquake recurrence along the Serghaya branch of the Dead Sea fault system in Syria and Lebanon. Geophysical Journal International 153, 658–674.

Gomez, F., Khawlie, M., Tabet, C., Darkal, A.N., Khair, K., Barazangi, M., 2006. Late Cenozoic uplift along the northern Dead Sea transform in Lebanon and Syria. Earth and Planetary Science Letters 241, 913–931.

Griffiths, H.M., Clark, R.A., Thorp, K.M., Spencer, S., 2000. Strain accommodation at the lateral margin of an active transpressive zone: geological and seismological evidence from the Lebanese restraining bend. Journal of the Geological Society, London 157, 289-302.

Hancock, P.L., Atiya, M.S., 1979. Tectonic significance of mesofracture systems associated with the Lebanese segment of the Dead Sea transform fault. Journal of Structural Geology 1, 143–153.

Joffe, S., Garfunkel, Z., 1987. Plate kinematics of the circum Red Sea — a re-evaluation. Tectonophysics 141, 5–22.

Khair, K., 2001. Geomorphology and seismicity of the Roum fault as one of the active branches of the Dead Sea fault system in Lebanon. Journal of Geophysical Research 106, 4233–4245.

McBride, J.H., Barazangi, M., Best, J., Al-Saad, D., Sawaf, T., Al-Otri, M., Gebran, A., 1990. Seismic reflection structure of Intracratonic Palmyride Fold-Thrust belt and surrounding Arabian Platform, Syria. American Association of Petroleum Geologists Bulletin 74, 238–259.

McClusky, S., Reilinger, R., Mahmoud, S., Ben Sari, D., Tealeb, A., 2003. GPS constraints on Africa (Nubia) and Arabia plate motions. Geophysical Journal International 155, 126–138.

Meghraoui, M., Gomez, F., Sbeinati, R., van der Woerd, J., Mouty, M., Darkal, A.N., Radwan, Y., Layyous, I., Al-Najjar, H., Darawcheh, R., Hijazi, F., Al-Ghazzi, R., Barazangi, M., 2003. Evidence for 830 years of seismic quiescence from palaeoseismology, archaeoseismology and historical seismicity along the Dead Sea fault in Syria. Earth and Planetary Science Letters 210, 35–52.

Morewood, N.C., Roberts, G.P., 2002. Surface observations of active normal fault propagation: implications for growth. Journal of the Geological Society, London 159, 263-272.

Nemer, T., 2005. Sismotectonique et comportement sismique du relais transpressif de la faille du Levant: rôles et effets des branches de failles sur l'aléa sismique au Liban. PhD thesis, Université Louis Pasteur, Strasbourg.

Plassard, J., Kogoj, B., 1981. Seismicité du Liban. Annales Memoires de l'Observatoire de Ksara, v.4 (Sismologie), cah.1, 3ème edition. CNRS, Beyrouth.

Poirier, J., Taher, M., 1980. Historical seismicity in the Near and Middle East, North Africa, and Spain from Arabic documents (VIIth–XVIIIth century). Bulletin of the Seismological Society of America 70, 2185–2201.

Quennell, A.M., 1958. The structural and geomorphic evolution of the Dead Sea rift. The Quarterly Journal of the Geological Society of London 114, 1–24.

Sbeinati, M.R., Darawcheh, R., Mouty, M., 2005. The historical earthquakes of Syria: an analysis of large seismic events from 1365 B.C. to 1900 A.D. Annals of Geophysics 48, 347–435.

Stuiver, M., Reimer, P.J., 1993. Extended $^{14}C$ database and revised CALIB radiocarbon calibration program. Radiocarbon 35, 215–230.

Stuiver, M., Reimer, P.J., Bard, E., Beck, J.W., Burr, G.S., Hughen, K.A., Kromer, B., McCormac, G., van der Plicht, J., Spurk, M., 1998. INTCAL98 radiocarbon age calibration, 24000-0 cal BP. Radiocarbon 40, 1041–1083.

Wells, D., Coppersmith, K., 1994. New empirical relationships among magnitude, rupture length, rupture width, rupture area, and surface displacement. Bulletin of the Seismological Society of America 84, 974–1002.

Yeats, R.S., Sieh, K., Allen, C.R., 1997. The Geology of Earthquakes. Oxford University Press.